

VIP Very Important Paper

www.batteries-supercaps.org

# High-Performance Zinc-Ion Battery Enabled by Tuning the Terminal Group and Chain Length of PEO-based Oligomers

Min Yu<sup>+[a]</sup> ShunShun Zhao<sup>+[b]</sup> Ying Xiao,<sup>[b]</sup> Ruixin Zhang,<sup>[a]</sup> Lili Liu,\*<sup>[a]</sup> and Shimou Chen,\*<sup>[b]</sup>

Side reactions and dendrite growth issues originated from free water seriously hamper the application of zinc-ion batteries (ZIB). The electrolyte strategy of using a co-solvent system has been proven to effectively improve the performance of ZIB. However, lack of thorough understanding of the co-solvent structure on the performance of electrolytes hinders the rational design of co-solvent electrolytes. Here, by studying how the terminal group and chain length of polyethylene oxide (PEO)

based oligomers affect the electrochemical performance of ZIB, we obtained the optimized PEO oligomer structure and the underlying mechanism. As a result, the designed co-solvent electrolyte enables the  $Zn||NH_4V_4O_{10}$  full cell to gain a 98.5% capacity retention over 9500 cycles at  $10\text{ A g}^{-1}$ . This work provides new insights into the inhibition of water-related side reactions and further promote the development of electrolytes for ZIB and other metal batteries.

## Introduction

The rechargeable aqueous batteries have the advantages of excellent safety, relatively low cost and environmental friendliness, which are expected to meet the increasing demand for next generation electrochemical energy storage systems.<sup>[1]</sup> Among them, aqueous zinc-ions batteries (ZIB) attract much attention, due to the volume specific capacity of the metal zinc is up to  $5855\text{ mAh cm}^{-3}$ , and its mass specific capacity is up to  $820\text{ mAh g}^{-1}$ . In addition, the zinc metal has a low redox potential ( $-0.76\text{ V}$  relative to the standard hydrogen electrode). Therefore, metal zinc is a particularly promising anode material.<sup>[2]</sup> Unfortunately, the problems with Zn anodes including water-induced dendrite growth and side reactions still hampered the commercial application of rechargeable aqueous ZIB. Generally, the corrosion of the Zn anode and continuous consumption of the electrolyte during cycling are the main side reactions, and dendrite growth originates from tip growth driven by the non-uniform distribution of  $Zn^{2+}$  on the anode.<sup>[3]</sup>

In recent years, in order to solve the above obstacles, numerous solutions have been proposed by researchers, such as tuning the salt concentration,<sup>[4]</sup> using deep eutectic electrolyte,<sup>[5]</sup> and co-solvent strategy<sup>[6]</sup> etc. However, concentrated salt electrolyte and deep eutectic electrolyte have the

inherent drawbacks of high price and limited ionic conductivity. In contrast, the co-solvent strategy has lately gained popularity due to its low cost, ease of operation, and high efficiency to reduce water reactivity.<sup>[7]</sup> Different organic co-solvents (for example, dimethyl sulfoxide, methanol, and ethylene glycol)<sup>[6b,8]</sup> have been used to create hydrogen bonds (H-bonds) with  $H_2O$ , to further disrupt the hydrogen bond network structure between  $H_2O-H_2O$  molecules, hence suppress water-induced parasitic processes. In addition, some of the co-solvent can preferentially immobilized on the Zn surface to isolate the water adsorption, which can suppress the parasitic reaction induced by water.<sup>[9]</sup> Although great success has been achieved in co-solvent electrolyte, the influence of co-solvent structure on the key performance of electrolyte is not fully understood, which hinders the reasonable design of co-solvent electrolyte for high-performance ZIB.

In this research, we systematically examined different terminal groups and different chain lengths of the PEO-based oligomers to study their influences on the co-solvent electrochemical properties. We focused on the  $H_2O$ -oligomers intermolecular interactions and the key performance of electrolyte. The experimental results show that the interaction between the oligomers can be tuned by regulating their terminal groups, and the weak interaction between the oligomers can inhibit the activity of water, thus stabilizing the Zn anode. In addition, the reaction kinetics was optimized by regulating the chain length to achieve the optimal adsorption of Zn anode, to protect the Zn anode and prolong the battery life. Finally, we formulated an optimal structure of polyethylene glycol dimethyl ether (PEGDME) with a molecular weight of 375 (named as PEGDME375). The optimized PEGDME375-based aqueous electrolyte can effectively inhibit the activity of water and stabilize the Zn anode, which can support symmetrical  $Zn||Zn$  cell to cycle for 500 h at large currents of  $10\text{ mA cm}^{-2}$ . The electrolyte also can support the  $Zn||NVO$  full cell, which could retain 98.5% of its initial capacity after 9500 cycles at  $10\text{ A g}^{-1}$ .

[a] M. Yu,<sup>+</sup> R. Zhang, Dr. L. Liu  
College of Chemistry and Materials Engineering  
Beijing Technology and Business University  
Beijing, 100048 (China)  
E-mail: liulili@bjtu.edu.cn

[b] S. Zhao,<sup>+</sup> Dr. Y. Xiao, Prof. S. Chen  
State Key Laboratory of Chemical Resource Engineering  
Beijing Key Laboratory of Electrochemical Process and Technology of Materials  
College of Materials Science and Engineering  
Beijing University of Chemical Technology  
Beijing, 100029 (China)  
E-mail: chensm@buct.edu.cn

<sup>[+]</sup> These authors contributed equally to this work.

Supporting information for this article is available on the WWW under  
<https://doi.org/10.1002/batt.202200535>

## Results and Discussion

In this study, three types of PEO-based oligomers with different terminal groups (PEGDA, PEG, and PEGDME) were investigated to disclose how the oligomer structure effect on the water reactivity (Figure 1a). The hybrid electrolytes were prepared by mixing different oligomers with deionized water at a volume ratio of 30:70, and then dissolving 2 M Zn(OTF)<sub>2</sub> in the hybrid solvent, and then labeling the electrolytes with PEG, PEGDA, PEGDME as PGZE, PAZE and PEZE, respectively. For comparison, 2 M Zn(OTF)<sub>2</sub> electrolyte without oligomer was used as the baseline electrolyte (simplified as BE). Figure 1(a) shows the structural formula of PEGDA, PEG, and PEGDME, whose backbone consists of multiple ether bonds. The backbone of PEG, PEGDME and PEGDA are all composed of  $(\text{CH}_2\text{CH}_2\text{O})_n$ , compared with PEG, PEGDME replaces the terminal H with an inert methyl group. PEGDA has a more complex terminal group, consisting of ester groups and double bonds. The interaction between molecules is different due to the different terminal groups.<sup>[10]</sup> Weakening the intermolecular interaction of molecules could effectively reduce the viscosity and achieve high ionic conductivity.<sup>[11]</sup>

Figure 1(b) shows that the viscosity order is PEG400 (92.6 mPa s) > PEGDA400 (56.1 mPa s) > PEGDME500 (33.5 mPa s) > PEGDME250 (4.45 mPa s), the number after the caps means the molecular weight of the oligomer. Figure 1(c) shows that the conductivity order is BE (60 mS cm<sup>-1</sup>) > PGZE (40.6 mS cm<sup>-1</sup>) > PAZE (32.9 mS cm<sup>-1</sup>) > PGZE (15.8 mS cm<sup>-1</sup>). This result shows that the inert end group reduces the viscosity. It is generally believed that the lower the average molecular weight, the lower the viscosity.<sup>[12]</sup> The viscosity of PEGDME500 with a higher average molecular weight, is much smaller than that of PEG400 and PEGDA400, indicating that PEGDME has less intermolecular interaction.<sup>[13]</sup> However, when the interaction between oligomer and oligomer is weak, the interaction between water and oligomer is relatively strong, thus breaking the hydrogen bond in water and reducing the activity of water.<sup>[14]</sup> This claim is supported by FTIR, Raman, and NMR spectroscopy results (Figure 1). Figure 1(d) shows the O–H tensile vibrations of H<sub>2</sub>O in different electrolytes ranging from 3800 to 2800 cm<sup>-1</sup>, and the full spectra are shown in Figure S1.<sup>[15]</sup> This O–H peak progressively changes to higher frequencies with the addition of PEG, PEGDA, and PEGDME, demonstrating that the hydrogen bond force

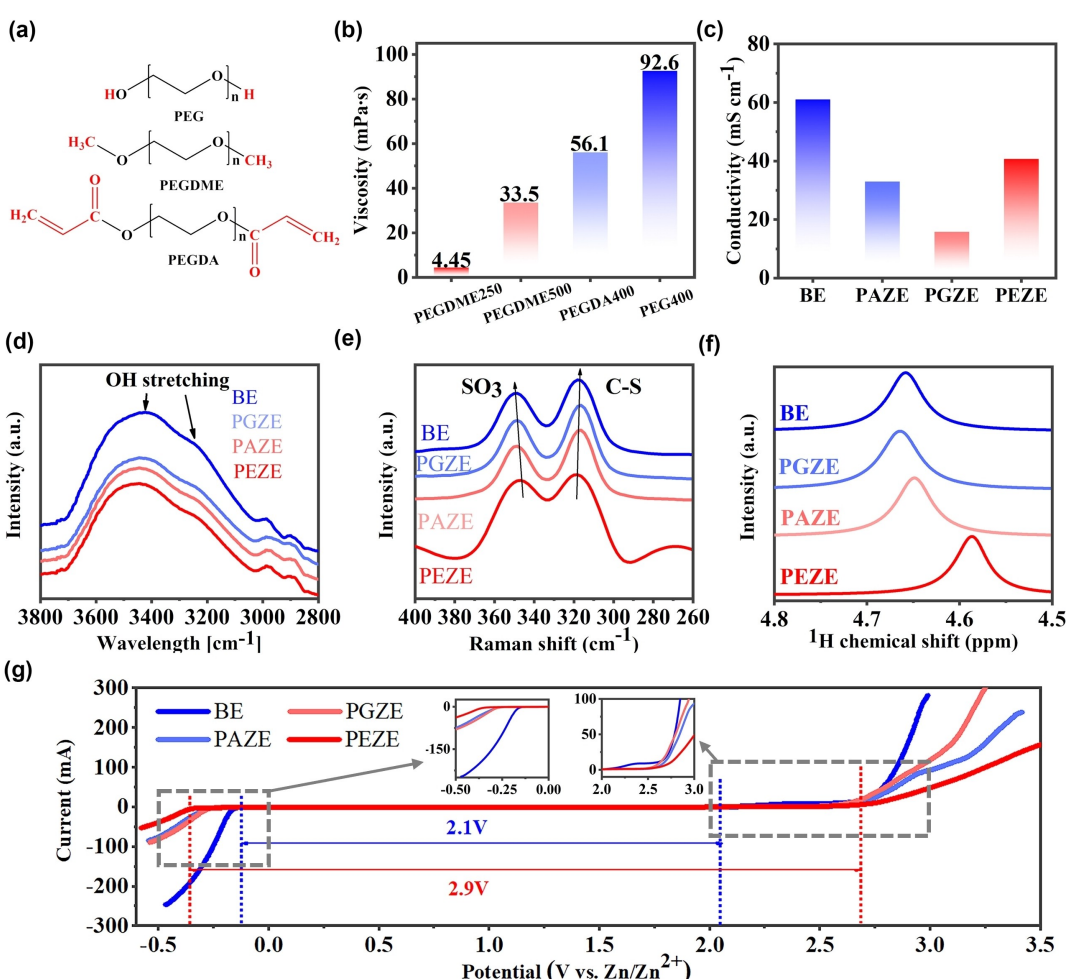


**Figure 1.** a) Structural formula of different oligomers. b) Viscosity of pure PEGDME250, PEGDME500, PEGDA400, and PEG400. c) Ionic conductivity of different electrolytes. d) FTIR spectra, e) Raman spectra and f) <sup>1</sup>H NMR spectra of different electrolytes. g) Electrochemical window of different electrolytes.

between the  $\text{H}_2\text{O}$  molecules in the electrolyte is weakened.<sup>[11]</sup> Additionally, the Raman spectra validate a very similar result (Figure 1e), with the introduction of PEGDME co-solvent, the sulfonyl group ( $-\text{SO}_3-$ ) stretching bands clearly exhibited a significant shift, which is ascribed to the enhanced interactions between the  $\text{OTF}^-$  and  $\text{Zn}^{2+}$ . This enhanced interaction is due to the strong solvation effect of PEGDME, which regulates the local solvation environment of zinc ions and reduces the number of coordinated water molecules.<sup>[7]</sup> Moreover, the strong interaction between the  $\text{OTF}^-$  and  $\text{Zn}^{2+}$  would weaken the electron absorption of the  $\text{Zn}^{2+}$  on water molecules, resulting in the higher LUMO energy level of  $\text{H}_2\text{O}$  in  $\text{Zn}^{2+}-\text{H}_2\text{O}-\text{OTF}^-$ -PEGDME complexes than in the  $\text{Zn}^{2+}-\text{H}_2\text{O}$  complexes, thus inhibiting the interfacial side reactions caused by  $\text{H}_2\text{O}$ .<sup>[16]</sup> Additionally,  $^1\text{H}$  NMR stability of the terminal ether bond also suggesting the existence of PEGDME can inhibit water-induced side reactions efficiently.<sup>[17]</sup>

Different terminal groups can widen the voltage window by influencing the interaction between water and oligomer. We performed linear sweep voltammetry (LSV) to determine the voltage window of different electrolytes (Figure 1g). Obviously, the electrochemical window of BE is 2.1 V, and with the addition of oligomer, the electrochemical window is enlarged in different degrees. The PEZE electrolyte makes the electrochemical window extend to 2.9 V at the maximum,

which is due to the stability of the terminal ether bond, indicating PEGDME has good capacity to restrain side reactions caused by water.<sup>[18]</sup>

Pristine Zn sheets were immersed in BE and oligomer-containing electrolytes to study how different oligomers corrode the Zn anode. The Zn sheets morphologies were analyzed by SEM after the Zn sheets soaked for 14 days at room temperature (Figure 2a-d). In the electrolyte containing PEZE, the Zn sheets have a glabrous and thick surface compared to the original zinc sheets, with no detectable  $\text{Zn}_x\text{OTf}_y(\text{OH})_{2x-y}\text{nH}_2\text{O}$ .<sup>[19]</sup> However, for the Zn sheets soaked in PGZE and PAZE, rough surfaces were obtained. The zinc symmetrical batteries were employed to investigate the electrochemical stability of Zn electrodes in electrolytes containing different oligomers at 5  $\text{mA cm}^{-2}$ . The cycle time of the Zn anode prolonged considerably with the addition of oligomer, demonstrating that the oligomer enhance the Zn stability by breaking hydrogen bond network and suppressing water-involved side reactions.<sup>[7,8b,19a]</sup> The battery containing PEZE electrolyte has the longest lifetime (over 500 h, Figure 2e). Figure S2 provides the amplified voltage curve. Furthermore, the Coulombic efficiencies (CE) obtained in different oligomers-water co-solvents demonstrate the superiority of electrolytes. Figure 2(f) depicts the CE of  $\text{Zn}||\text{Cu}$  batteries at 1  $\text{mA cm}^{-2}/1 \text{mAh cm}^{-2}$  in different electrolytes.

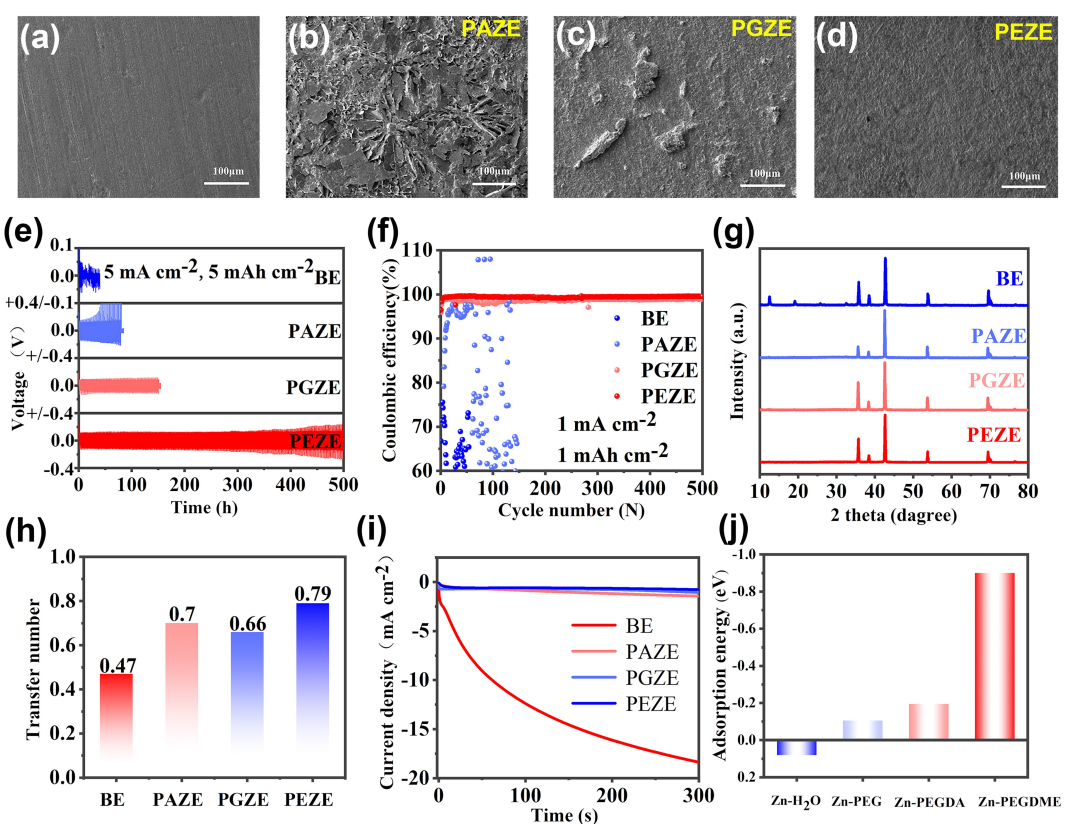


**Figure 2.** SEM images of zinc plate initially and after 14 days of immersion in different electrolytes. a) initial, b) PAZE, c) PGZE, and d) PEZE. e) Time-voltage curves of  $\text{Zn}||\text{Zn}$  batteries in different electrolytes with 5  $\text{mA cm}^{-2}/5 \text{mAh cm}^{-2}$ . f) Coulombic efficiencies of  $\text{Zn}||\text{Cu}$  batteries in different electrolytes at 1  $\text{mA cm}^{-2}/1 \text{mAh cm}^{-2}$ . g) XRD patterns of Zn anodes after 50 cycles at 2  $\text{mA cm}^{-2}/2 \text{mAh cm}^{-2}$  in different electrolytes. h)  $\text{Zn}^{2+}$  transfer number in different electrolytes. i) CA curves of  $\text{Zn}||\text{Zn}$  batteries in different electrolytes at -150 mV. j) The adsorption energy of  $\text{H}_2\text{O}$ , PEG, PEGDA, and PEGDME on the Zn(002) surface.

With the use of BE electrolyte, the first CE was 66.8% and the average CE was about 62.6% for 54 cycles. The CE of using PAZE electrolyte also not satisfied, the first CE is 71.2%, even though the CE reaches to 95.1% for 59 cycles, it began to fluctuate sharply in the subsequent cycles, indicating serious side reactions happened. The PGZE and PEZE electrolytes achieved high first CE of 95.8% and 96.4%, respectively, and higher average CE of 98.1% and 99.5% after 1000 cycles. More notably, as illustrated in Figures S3 and S4, the PEZE electrolyte has more visible benefits in the CE at  $5\text{ mA cm}^{-2}$ /  $5\text{ mAh cm}^{-2}$ .

To analyze the composition of zinc sheet, X-ray diffraction (XRD) characterization was performed, the result reveal that the cycled Zn electrode in BE has additional peaks at  $13.2^\circ$ ,  $19.3^\circ$  and  $26.8^\circ$ , which assigned to the byproduct of  $\text{Zn}_x\text{OTf}_y\cdot(\text{OH})_{2x-y}\cdot n\text{H}_2\text{O}$  generated by the strong HER side reaction (Figures 2g and S5). By comparison, the peaks related to byproducts is hardly detectable in PAZE, PGZE, and PEZE electrolytes, showing a good effect of inhibiting side reactions. Among them, PEZE electrolyte has the most obvious effect.

The ion transference number was calculated by using electrochemical impedance spectroscopy (EIS) (Figures 2h and S6). The order of transference number is PEZE (0.79) > PAZE (0.70) > PGZE (0.66) > BE (0.47), which proves that the water-oligomer co-solvent strategy is also beneficial to zinc ion migration, and the PEZE electrolyte has the best effect.<sup>[20]</sup> Chronoamperometry (CA) was employed to investigate the influence of different oligomers on Zn deposition (Figure 2i). The growing current density in BE implies that 2D diffusion of  $\text{Zn}^{2+}$  occurs on the Zn electrodes, which will contribute to the Zn dendrite growth. However, in the oligomers-water co-solvent system, the current density was very stable, indicating that the 2D diffusion of  $\text{Zn}^{2+}$  in the system was blocked.<sup>[21]</sup> The order of current density is PEZE, PGZE, PAZE, which further indicates that PEGDME is the most effective electrolyte for stabilizing the Zn anode. Furthermore, the interaction between the Zinc (002) surface and the oligomer was investigated by density functional theory (DFT) theoretical calculations.<sup>[22]</sup> The priority of oligomers adsorption on the Zn surface is indicated by the fact that all three oligomers have higher absorption energy than  $\text{H}_2\text{O}$ , as shown in Figure 2(j). Furthermore, PEGDME has the highest adsorption energy ( $-0.9\text{ eV}$ ), indicating that PEGDME can preferentially adsorb on zinc surface to isolate water adsorption and block HER. Based on the theoretical calculations, it is found that PEGDME with inert methyl group has the strongest damaging effect on the hydrogen-bond network of water, which can greatly reduce the water activity.

According to the above analysis, we choose PEGDME as the co-solvent to examine how chain length affects the efficiency of the electrolyte, and a series of PEGDME with different molecular weight were employed, such as PEGDME250,

PEGDME300, PEGDME375, PEGDME450, PEGDME500 (Table S1).<sup>[23]</sup> The prepared PEGDME-water co-solvent electrolytes are denoted as PE<sub>250</sub>, PE<sub>300</sub>, PE<sub>375</sub>, PE<sub>450</sub>, and PE<sub>500</sub>,

respectively. Figure 3(a) displays the ionic conductivity of several electrolytes, which diminishes progressively as the chain length grows. On the contrary, as shown in Figure 3(b), the viscosity gradually increases with the increase of the chain length.<sup>[24]</sup> Using the five electrolytes, we assembled Zn | Zn cells, the SEM images and XRD patterns of the zinc electrodes after cycling were examined to investigate the performance of the electrolyte. Figures 3(c) and S7 display the XRD patterns after 50 cycles, the intensity of the peaks of the byproduct  $\text{Zn}_x\text{OTf}_y\cdot(\text{OH})_{2x-y}\cdot n\text{H}_2\text{O}$  decreases first and then increases as the chain length increases, and the minimum intensity peak is obtained in the PE<sub>375</sub> electrolyte, indicating that the PE<sub>375</sub> electrolyte could inhibit the side reaction to the greatest extent.<sup>[25]</sup> Figure 3(d-h) shows SEM images after Zn anode cycling (see Figure S8 for SEM images at different magnifications). Which also clearly shows that a smooth Zn deposition obtained in the PE<sub>375</sub> electrolyte (Figure S9). However, if the chain length of the PEGDME is too long or too short, the rough surface of Zn deposition will appear.<sup>[26]</sup>

Using zinc symmetrical batteries at  $5\text{ mA cm}^{-2}/5\text{ mAh cm}^{-2}$  (Figure 3i) and  $10\text{ mA cm}^{-2}/10\text{ mAh cm}^{-2}$  (Figure 3j), the electrochemical stability of Zn anodes in five PEGDME-water electrolytes systems were evaluated. Figure S10 depicts the voltage curves of Zinc symmetrical cells at  $5\text{ mA cm}^{-2}/5\text{ mAh cm}^{-2}$ . We arrived a similar conclusion: as the chain length increase, the cycling time of the Zn anode first increased and then decreased, the PE<sub>375</sub> electrolyte having the longest lifetime (Over 800 hours). Which should be due to the PEGDME375 has the optimal structure for immobilizing onto Zn surface, avoiding direct contact of free  $\text{H}_2\text{O}$  and the Zn. When the chain length of PEGDME is very long, the kinetics of  $\text{Zn}^{2+}$  in the electrolyte is relative slow due to the high viscosity,<sup>[27]</sup> if the chain length is very short, it cannot isolate water from contacting Zn anode completely. Based on above results and consideration, we selected the PE<sub>375</sub> electrolyte for the following studies.

The cyclic stability of the Zn anode in PE<sub>375</sub> was further assessed at  $1\text{ mA cm}^{-2}/1\text{ mAh cm}^{-2}$ , showing over 3600 h of stable plating/stripping (Figure. 4a), Superior to those achieved in BE and previously reported mixed organic/aqueous electrolytes. We also investigated the CE of PE<sub>375</sub> at  $10\text{ mA cm}^{-2}/10\text{ mAh cm}^{-2}$  (Figure 4b). Surprisingly, it had an initial CE of 98% and maintained an average CE of 99.5% over the next 160 cycles. The voltage polarization curve (Figure 4c) also confirms its remarkable reversibility, which should be due to PEGDME375 has an outstanding capacity to restrain Zn dendrite growth and suppress water-involved side reactions. We also observed the in situ Zn plating processes in BE and PE<sub>375</sub> at  $5\text{ mA cm}^{-2}$  using an optical microscope. In the BE electrolyte, the Zn dendrite grows quickly (Figure 4d). However, in the PE<sub>375</sub> electrolyte, the Zn deposition layer presents a uniform and dense morphology (Figure 4e),<sup>[28]</sup> and no uneven deposition occurs after 60 min, which indicates that PE<sub>375</sub> achieves the uniform distribution of  $\text{Zn}^{2+}$  at the surface of Zn anode, and thus inhibits dendrite growth.

In Zn | PEZE | NVO full cells, the applicability of PEGDME-water electrolytes was further estimated.<sup>[20,29]</sup> In different

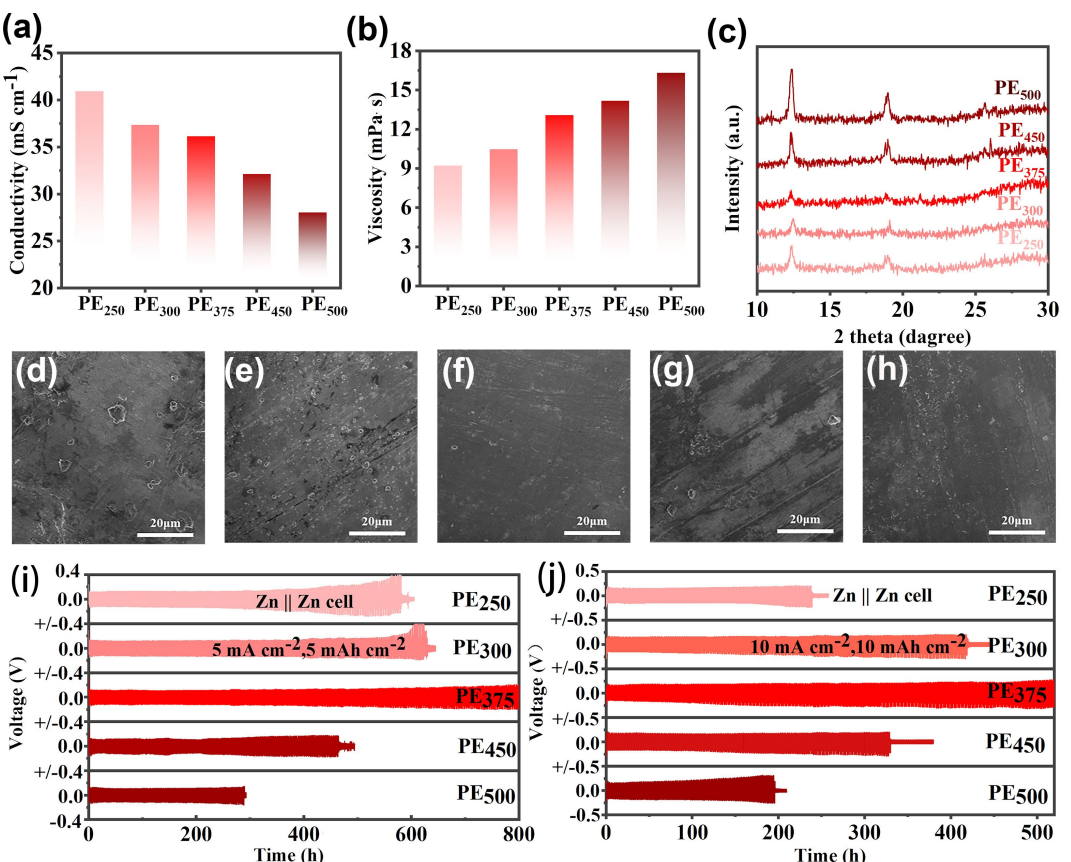


**Figure 3.** a) Ionic conductivity and b) viscosité of different electrolytes. c) XRD pattern and d-h) SEM images of Zn electrodes in the different electrolytes after 50 cycles at  $2 \text{ mA cm}^{-2}/2 \text{ mAh cm}^{-2}$ . i and j) Time-voltage curves of  $\text{Zn}||\text{Zn}$  batteries in different electrolytes at  $5/10 \text{ mA cm}^{-2}$  and  $5/10 \text{ mAh cm}^{-2}$ .

electrolytes, the rate capacity of  $\text{Zn}||\text{NVO}$  batteries was compared (Figure 5a). The battery containing PEZE shows best rate performance at current density from  $0.5$  to  $10 \text{ Ag}^{-1}$ . Figures S11, S12, and 5(b) further compare the cyclic voltammetry (CV) curves of  $\text{Zn}||\text{NVO}$  in different electrolytes. Compare to the curve of  $\text{Zn}||\text{PEZE}||\text{NVO}$  battery, the curves obtained from  $\text{Zn}||\text{BE}||\text{NVO}$  and  $\text{Zn}||\text{PAZE}||\text{NVO}$  batteries show much weaker intensities of oxidation/reduction peaks, indicating that NVO in these two batteries become inactive during cycling (Figure S12). Furthermore, the CV curves recorded in  $\text{Zn}||\text{PEZE}||\text{NVO}$  batteries after different cycles show identical features, demonstrating the excellent reversibility and electrochemical stability of the NVO electrodes in PEZE (Figure 5b). The peak intensity of the CV curves obtained in  $\text{Zn}||\text{PEZE}_{250}||\text{NVO}$  and  $\text{Zn}||\text{PEZE}_{500}||\text{NVO}$  cells also much lower than that of  $\text{Zn}||\text{PEZE}_{375}||\text{NVO}$  batteries (Figure S11).

In order to check the co-solvent electrolytes can stabilize cathode or not, after soaking the NVO positive plate into different electrolytes for 14 days, ICP tests performed to the four electrolytes, respectively (Figure 5c). It was found that the concentration of vanadium in PEZE electrolyte reached the minimum value, indicating that the PEZE could inhibit the positive electrode dissolution efficiently. The cycling stability of the  $\text{Zn}||\text{PEZE}_{375}||\text{NVO}$  cells is shown in Figure 5(d and e). The reversible capacity of the  $\text{Zn}||\text{PEZE}_{375}||\text{NVO}$  cells was up to  $482.4 \text{ mAh g}^{-1}$  at  $0.5 \text{ Ag}^{-1}$  after 200 cycles (Figure 5d). More

impressive is the  $\text{Zn}||\text{PEZE}_{375}||\text{NVO}$  battery maintained 100% capacity retention at  $5 \text{ Ag}^{-1}$  after 3000 cycles; it achieved a reversible capacity of up to  $302.8 \text{ mAh g}^{-1}$  (Figure 5e). As shown in Figure 5(f), we also test the cycling performances of  $\text{Zn}||\text{NVO}$  full cells at  $10 \text{ Ag}^{-1}$ . The  $\text{Zn}||\text{PEZE}_{375}||\text{NVO}$  battery maintained capacity retention to 98.5% after 9500 cycles, which much better than using electrolytes. Even compared with the previously reported similar aqueous zinc ion batteries (Figure 5g and Table 1),<sup>[5b,6,8,9,17,19a,30]</sup> by using the optimized co-solvent electrolyte obtained in this work, the  $\text{Zn}||\text{PEZE}_{375}||\text{NVO}$  cells showed more excellent electrochemical stability and better reversibility.

## Conclusion

In summary, we designed a cheap and efficient PEO-based oligomer and water co-solvents electrolyte to reduce the free  $\text{H}_2\text{O}$  and restrain the side reactions of the Zn anode. The terminal group and chain length of PEO-based oligomers show big influence on the electrolyte performance. Experimental and theoretical studies demonstrate that PEGDME375 oligomer may stabilize Zn anode in two ways, including i) the PEGDME375 forms hydrogen bonds with  $\text{H}_2\text{O}$  to change the hydrogen bond network in the electrolyte, ii) the PEGDME375 is preferably adsorbed on the surface of zinc sheets to restrain

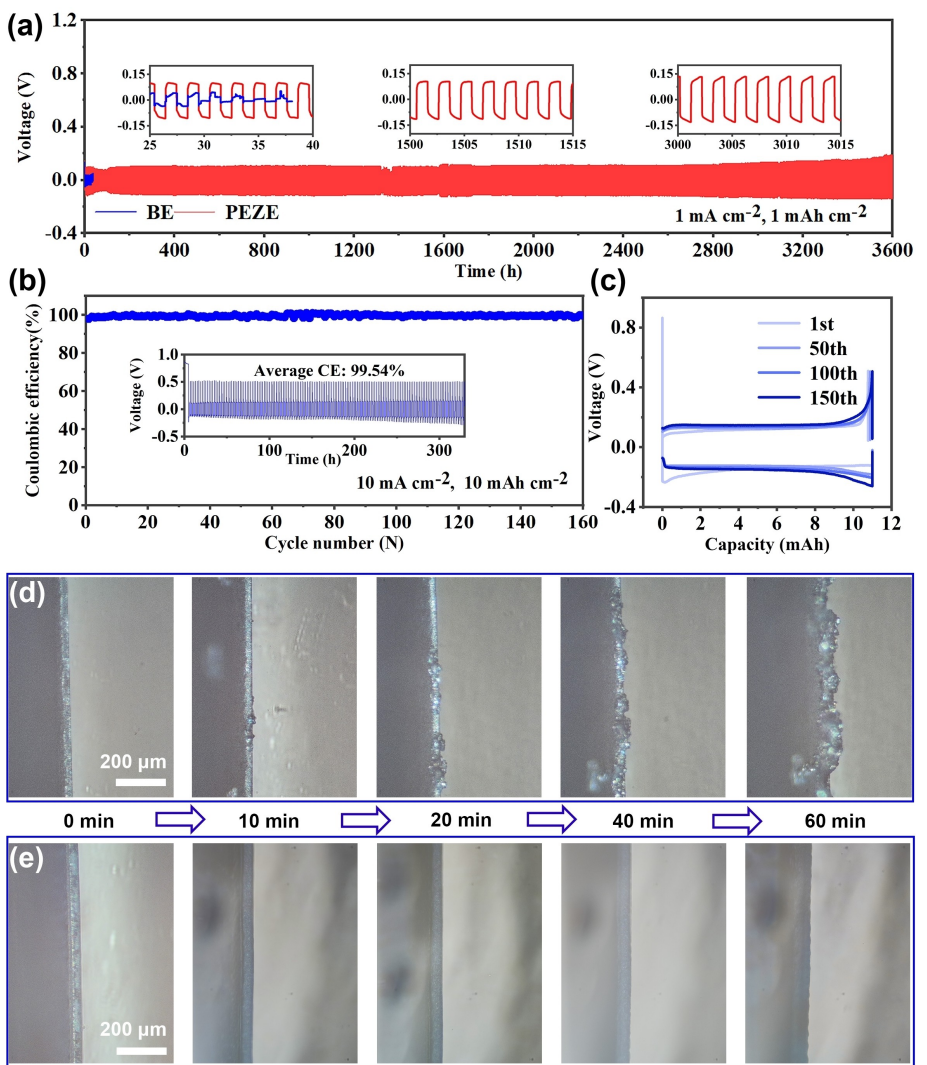


**Figure 4.** a) Time-voltage curves of  $\text{Zn} \parallel \text{Zn}$  batteries in different electrolytes at  $1 \text{ mA cm}^{-2}/1 \text{ mAh cm}^{-2}$ . b) Coulombic efficiencies in PEZE at  $10 \text{ mA cm}^{-2}/10 \text{ mAh cm}^{-2}$ . c) The corresponding voltage polarization profiles after different cycles at  $10 \text{ mA cm}^{-2}/10 \text{ mAh cm}^{-2}$  in PEZE. Zn plating images taken under an optical microscope in real time in d) BE and e) PEZE.

the corrosion of zinc anode by  $\text{H}_2\text{O}$ . The optimized co-solvent electrolyte not only increased zinc plating/stripping stability up to 500 hours at  $10 \text{ mA cm}^{-2}/10 \text{ mAh cm}^{-2}$ , but also demonstrated great reversibility, its average CE is up to 99.5% for 1000 cycles at  $1 \text{ mA cm}^{-2}/1 \text{ mAh cm}^{-2}$ . It is also can support the  $\text{Zn} \parallel \text{NVO}$  full cell with long lifespan, up to 98.5 % capacity retention at  $10 \text{ A g}^{-1}$  after 9500 cycles was obtained. Our work provides a new viewpoint for designing high performance electrolyte for zinc-ion batteries, and may shed light on exploration of PEO-base oligomers in other aqueous metal batteries.

## Experimental Section

### Materials

Poly(ethylene glycol) dimethyl ether (PEGDME, Mn250, Mn500), poly(ethylene glycol) (PEG, Mn400), polyethylene (glycol) diacrylate (PEGDA,  $M_n \approx 400$ ), Zinc trifluoromethanesulfonate ( $\text{Zn}(\text{OTF})_2$ , 98 %), Zinc foil (> 99.9%, 70  $\mu\text{m}$  thickness), copper foil (> 99.9%, 50  $\mu\text{m}$  thickness), stainless steel mesh (316, 500 mesh), Glass microfiber filters (Whatman GF/D).

### Fabrication of $\text{NH}_4\text{V}_4\text{O}_{10}$ (NVO) cathode materials

Firstly, 240 mL of deionized water was heated to 80 °C, and 3.510 g of  $\text{NH}_4\text{VO}_3$  solid powder was added. Secondly, 5.673 g  $\text{H}_2\text{C}_2\text{O}_4 \cdot 2\text{H}_2\text{O}$  was added when the solution was yellow. Finally, when the solution became dark blue, the solution was transferred to a Teflon reaction kettle, which heated at 140 °C for 48 hours. The resulting products were washed completely by anhydrous alcohol and deionized water. Then it was dried in a vacuum drying chamber at 80 °C for 12 h to obtain the final  $\text{NH}_4\text{V}_4\text{O}_{10}$  solid powder. To prepare

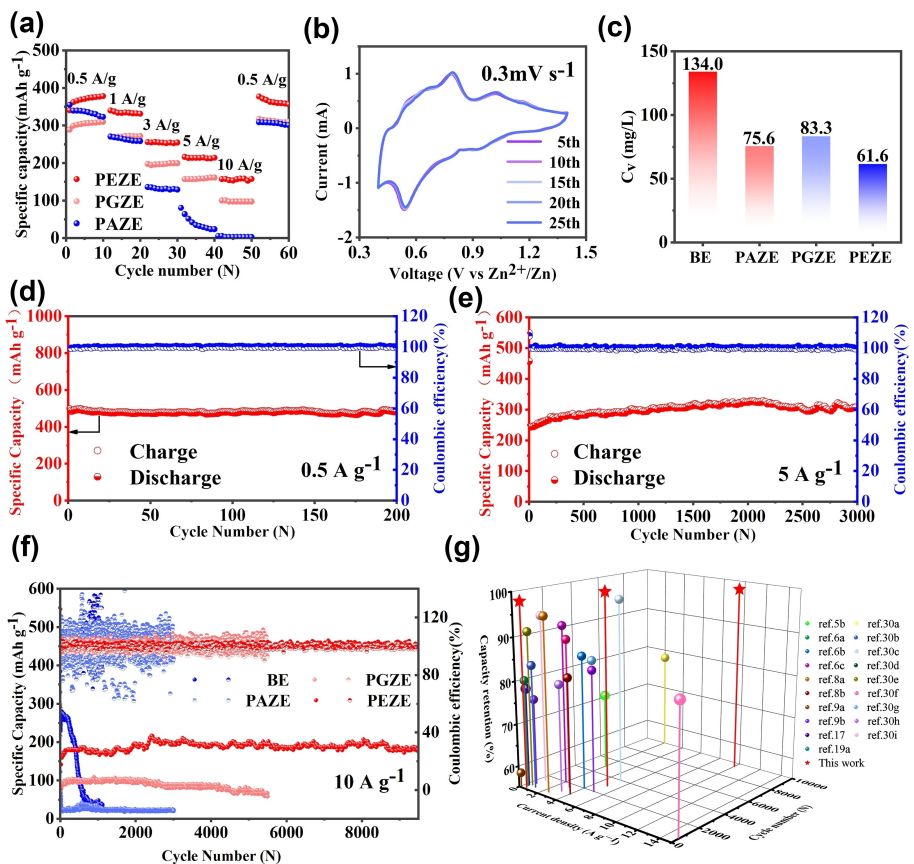


**Figure 5.** a) The rate performances of Zn||NVO cells in different electrolytes. b) CV curves of the Zn||NVO batteries in PEZE. c) The concentration of V was tested by ICP. The cycling performance of Zn||NVO batteries in PEZE at a current density of d) 0.5 A g<sup>-1</sup>, e) 5 A g<sup>-1</sup>. f) The cycling performance of Zn||NVO batteries in the four electrolytes at 10 A g<sup>-1</sup>. g) Comparison of cycling performance, current density, and capacity retention of the batteries in this work and other reported literatures.

**Table 1.** Comparison of capacity retention, current density, and cycle number between this work and the previous ones.

Cathode material	Electrolyte	Capacity [mAh g <sup>-1</sup> ]	Current density [mA g <sup>-1</sup> ]	Cycle number	Capacity retention	Ref.
V <sub>2</sub> O <sub>5</sub>	70%PEG400 in 1 M Zn(OTF) <sub>2</sub>		15000	500	84%	[30e]
PANI/CF	1 m G4 in 2 M Zn(OTF) <sub>2</sub>	145.2	500	1500	94%	[19a]
LiMn <sub>2</sub> O <sub>4</sub>	10%PG in 1 M ZnSO <sub>4</sub>	300	500	78%	[30g]	
VO <sub>2</sub>	Na <sub>4</sub> EDTA in 1 M ZnSO <sub>4</sub>	120	4000	2000	86%	[30c]
MnO <sub>2</sub>	Glucose in 1 M ZnSO <sub>4</sub>	3080	1000	80%	[17]	
PANI	Anti-M-50% in 2 M ZnSO <sub>4</sub>	114.6	5000	2000	85.5%	[6b]
MnO <sub>2</sub>	2 vol% Et <sub>2</sub> O in 3 M Zn(OTF) <sub>2</sub>	113	5000	4000	97.7%	[30d]
NaV <sub>3</sub> O <sub>8</sub> ·1.5H <sub>2</sub> O	1 M Na <sub>2</sub> SO <sub>4</sub> in 1 M ZnSO <sub>4</sub>	4000	1000	82%	[30f]	
LiMn <sub>2</sub> O <sub>4</sub>	0.5 wt% PEO in 1 M ZnSO <sub>4</sub>	75	100	58.3%	[9b]	
MnO <sub>2</sub>	ZnCl <sub>2</sub> –H <sub>2</sub> O–DMSO	150.3	2464	500	95.3%	[8b]
V <sub>2</sub> O <sub>5</sub> ·nH <sub>2</sub> O	7 m DEC in 2 M Zn(OTF) <sub>2</sub>	202	2000	5000	72.9%	[9a]
PANI	EG–ZnCl <sub>2</sub>		2000	10000	78%	[8a]
NH <sub>4</sub> V <sub>4</sub> O <sub>10</sub>	HEE-1,2-3	500	600	91%	[5b]	
LFP	ZSO/Ce	338	400	80%	[30a]	
Od-NVO	NH <sub>4</sub> OAc-added electrolytes	1000	500	83.7%	[30i]	
MnO <sub>2</sub>	ZnSO <sub>4</sub> + 10%DMA	188	500	880	75.2%	[6a]
V <sub>2</sub> O <sub>5</sub>	ZnSO <sub>4</sub> –CHD	175	2000	2000	92%	[30b]
NH <sub>4</sub> V <sub>4</sub> O <sub>10</sub>	Zn–PG		5000	2000	83.3%	[30 h]
V <sub>2</sub> O <sub>5</sub> ·1.6H <sub>2</sub> O	45%PEG–Zn(OTF) <sub>2</sub>	213.9	3000	1600	89.6%	[6c]
Our NH <sub>4</sub> V <sub>4</sub> O <sub>10</sub>	PZEZ <sub>375</sub>	482.4	500	200	98%	
		302.8	5000	3000	100%	This work
		180.2	10000	9500	98.5%	

the cathode plate,  $\text{NH}_4\text{V}_4\text{O}_{10}$ , Ketjen black, and polytetrafluoroethylene (PTFE) (60 w% aqueous solution) were mixed in a 7:2:1 weight ratio using absolute ethanol as solvent. The mixture was stirred evenly. The slurry was pressed into a 500 mesh stainless steel net using a roller press, cut into a small size of 12 mm in diameter, and dried under vacuum for 8 hours at 60°C. The effective mass loading is about 1.4–3.0 mg cm<sup>-2</sup>.

### Fabrication of electrolytes

PEGDME, PEG and PEGDA were mixed with deionized water at a volume ratio of 30:70, and then dissolving 2 M  $\text{Zn}(\text{OTF})_2$  in the hybrid solvent, and then labelling the electrolytes with PEG, PEGDA, PEGDME as PGZE, PAZE, PEZE, respectively. For comparison, 2 M  $\text{Zn}(\text{OTF})_2$  aqueous solution without oligomer was used as the baseline electrolyte (simplified as BE). The composition of the prepared PEGDME300, PEGDME375, PEGDME450 are shown in Table S1. The preparation procedure of PE<sub>250</sub>, PE<sub>300</sub>, PE<sub>375</sub>, PE<sub>450</sub> and PE<sub>500</sub> electrolytes is the same as above.

### Characterizations

The viscosity was measured using a viscosity density meter (DMA5000M-Lovis2000ME). The FTIR spectra were recorded on the Thermo IR200 spectrometer. The Raman spectra were recorded by an in Via reflection system with a 532 nm excitation laser. The <sup>1</sup>H NMR spectra were collected through a Bruker Advance 400. The morphology of zinc deposition on zinc anode was observed by a scanning electron microscope (SEM) (TESCAN, MAIA3 XMU). X-ray diffraction (XRD, D8 ADVANCE with Cu  $K_\alpha$ ,  $\lambda=0.15406$  nm) was used to study the crystal structure. In-situ optical images were obtained on an automatic focusing metallographic microscope (L302-AF516C) by an electrochemical cell with an optical window.

### Electrochemical measurements

The Zn||Zn batteries, Zn||Cu batteries, Zn||NVO batteries and Zn||SS batteries are CR2023 type coin batteries. The volume of electrolyte is 80 μl in each coin battery. The Zn||Zn cells used for measuring the battery life, CA, and transfer number. CA was performed at -150 mV for 300 seconds with an Autolab electrochemical workstation (PGSTAT302N). The  $\text{Zn}^{2+}$  transfer number was calculated from the I-T curves, and EIS was tested before and after the measurement. The frequency range of EIS test is 0.01–1 × 10<sup>5</sup> Hz, and the disturbance amplitude is 5 mV. The coulomb efficiency, CV, cycling performance of Zn||Cu cells and Zn||NVO cells were tested with LAND CT2001A equipment.

### Calculation methods

The commercial software, Vienna Ab-initio Simulation Package (VASP), was used to calculate the adsorption energy ( $E_{\text{ads}}$ ). The development of VASP software is based on density functional theory (DFT).<sup>[31]</sup> DFT based on quantum mechanics is a strict theory for solving single electron problems. In order to improve the calculation accuracy, we use the generalized gradient approximate functional. The plane-wave cutoff energy is 450 eV and the Brillouin zone is sampled in k-space using a Monkhorst-Pack scheme of 3 × 3 × 1. The structures of all the molecules are completely relaxed to the ground state, and the spin polarization is taken into account in the whole calculation. All computer simulations have convergence requirements of 10<sup>-5</sup> eV in energy and 0.02 eV/Å in force. The  $E_{\text{ads}}$  were calculated as:

$$E_{\text{ads}} = E_{\text{ab/sub}} - E_{\text{ad}} - E_{\text{sub}},$$

where  $E_{\text{ab/sub}}$  is the total energy after adsorption of organic molecules,  $E_{\text{ab}}$  is the energy of a single isolated organic molecule, and  $E_{\text{sub}}$  is the energy after the cutting plane of zinc metal.

### Acknowledgements

This work was supported financially by National Natural Science Foundation of China (52171198, 51922099), Innovation Academy for Light-duty Gas Turbine, Chinese Academy of Sciences (CXYJJ20-MS-05), Natural Science Foundation of Hebei Province for Distinguished Young Scholars (E2020103052), and School Level Cultivation Fund of Beijing Technology and Business University for Distinguished and Excellent Young Scholars.

### Conflict of Interest

The authors declare no conflict of interest.

### Data Availability Statement

The data that support the findings of this study are available from the corresponding author upon reasonable request.

**Keywords:** zinc-ion battery · electrolyte · co-solvent · PEO-base oligomers

- [1] a) F. Zhang, W. Zhang, D. Wexler, Z. Guo, *Adv. Mater.* **2022**, *34*, 2107965; b) W. Yang, Y. Yang, H. Yang, H. Zhou, *ACS Energy Lett.* **2022**, *7*, 2515–2530; c) Y. Lv, Y. Xiao, L. Ma, C. Zhi, S. Chen, *Adv. Mater.* **2022**, *34*, 2106409; d) X. Chen, P. Ruan, X. Wu, S. Liang, J. Zhou, *Acta Phys. Chim. Sin* **2022**, *38*, 2111003.
- [2] a) H. Dong, J. Li, J. Guo, F. Lai, F. Zhao, Y. Jiao, D. J. L. Brett, T. Liu, G. He, I. P. Parkin, *Adv. Mater.* **2021**, *33*, 2007548; b) L. Ma, S. Chen, N. Li, Z. Liu, Z. Tang, J. A. Zapien, S. Chen, J. Fan, C. Zhi, *Adv. Mater.* **2020**, *32*, 1908121.
- [3] a) Z. Yi, G. Chen, F. Hou, L. Wang, J. Liang, *Adv. Energy Mater.* **2021**, *11*, 2003065; b) Y. Song, P. Ruan, C. Mao, Y. Chang, L. Wang, L. Dai, P. Zhou, B. Lu, J. Zhou, Z. He, *Nano-Micro Lett.* **2022**, *14*, 218.
- [4] a) Y. Zhang, G. Wan, N. H. C. Lewis, J. Mars, S. E. Bone, H. G. Steinrück, M. R. Lukatskaya, N. J. Weadock, M. Bajdich, O. Borodin, A. Tokmakoff, M. F. Toney, E. J. Maginn, *ACS Energy Lett.* **2021**, *6*, 3458–3463; b) L. Sun, Y. Yao, L. Dai, M. Jiao, B. Ding, Q. Yu, J. Tang, B. Liu, *Energy Storage Mater.* **2022**, *47*, 187–194; c) C. Y. Li, M. Chen, S. Liu, X. Lu, J. Meng, J. Yan, H. D. Abruna, G. Feng, T. Lian, *Nat. Commun.* **2022**, *13*, 1–10.
- [5] a) X. Lin, G. Zhou, M. J. Robson, J. Yu, S. C. T. Kwok, F. Ciucci, *Adv. Funct. Mater.* **2022**, *32*, 2109322; b) M. Han, J. Huang, X. Xie, T. C. Li, J. Huang, S. Liang, J. Zhou, H. J. Fan, *Adv. Funct. Mater.* **2022**, *32*, 2110957; c) L. Ma, S. Chen, X. Li, A. Chen, B. Dong, C. Zhi, *Angew. Chem. Int. Ed. Engl.* **2020**, *132*, 24044–24052.
- [6] a) F. Wu, Y. Chen, Y. Chen, R. Yin, Y. Feng, D. Zheng, X. Xu, W. Shi, W. Liu, X. Cao, *Small* **2022**, *18*, 2202363; b) J. Hao, L. Yuan, C. Ye, D. Chao, K. Davey, Z. Guo, S. Z. Qiao, *Angew. Chem. Int. Ed. Engl.* **2021**, *60*, 7366–7375; c) Z. Cao, X. Zhu, S. Gao, D. Xu, Z. Wang, Z. Ye, L. Wang, B. Chen, L. Li, M. Ye, J. Shen, *Small* **2022**, *18*, 2103345.
- [7] Z. Hou, Z. Lu, Q. Chen, B. Zhang, *Energy Storage Mater.* **2021**, *42*, 517–525.
- [8] a) L. Geng, J. Meng, X. Wang, C. Han, K. Han, Z. Xiao, M. Huang, P. Xu, L. Zhang, L. Zhou, L. Mai, *Angew. Chem. Int. Ed. Engl.* **2022**, *134*,

- e202206717; b) L. Cao, D. Li, E. Hu, J. Xu, T. Deng, L. Ma, Y. Wang, X. Q. Yang, C. Wang, *J. Am. Chem. Soc.* **2020**, *142*, 21404–21409.
- [9] a) L. Miao, R. Wang, S. Di, Z. Qian, L. Zhang, W. Xin, M. Liu, Z. Zhu, S. Chu, Y. Du, N. Zhang, *ACS Nano* **2022**, *16*, 9667–9678; b) Y. Jin, K. S. Han, Y. Shao, M. L. Sushko, J. Xiao, H. Pan, J. Liu, *Adv. Funct. Mater.* **2020**, *30*, 2003932; c) A. Mitha, A. Z. Yazdi, M. Ahmed, P. Chen, *ChemElectroChem* **2018**, *5*, 2409–2418.
- [10] a) M. T. Zafarani-Moattar, H. Shekaari, P. Jafari, *J. Chem. Eng. Data* **2019**, *64*, 1322–1337; b) I. Khoiroh, S. Y. Lee, M. Pirdashti, M. J. Lee, *RSC Adv.* **2020**, *10*, 21760–21771.
- [11] D. S. Liu, Y. Zhang, S. Liu, L. Wei, S. You, D. Chen, M. Ye, Y. Yang, X. Rui, Y. Qin, C. C. Li, *Adv. Funct. Mater.* **2022**, *32*, 2111714.
- [12] J. A. Cintron-Cruz, B. R. Freedman, M. Lee, C. Johnson, H. Ijaz, D. J. Mooney, *Adv. Mater.* **2022**, *34*, 2205567.
- [13] E. Hanke, U. Schulz, U. Kaatze, *ChemPhysChem* **2007**, *8*, 553–560.
- [14] a) A. L. Sturlaugson, K. S. Fruchey, S. R. Lynch, S. R. Arago'n, M. D. Fayer, *Phys. Rev. B* **2010**, *114*, 5350–5358; b) A. Burakowski, J. Gliński, M. Riederer, *J. Mol. Liq.* **2019**, *276*, 179–183; c) D. Das Mahanta, D. Rana, A. Patra, B. Mukherjee, R. K. Mitra, *Chem. Phys. Lett.* **2018**, *700*, 50–56; d) G. M. Xu, X. X. Li, Y. J. Hu, Y. W. Wang, G. C. Fan, M. Zhang, *J. Chem. Eng. Data* **2010**, *55*, 2345–2348; e) D. Das Mahanta, S. I. Islam, S. Choudhury, D. K. Das, R. K. Mitra, A. Barman, *J. Mol. Liq.* **2019**, *290*, 111194.
- [15] Q. Zhang, Y. Ma, Y. Lu, L. Li, F. Wan, K. Zhang, J. Chen, *Nat. Commun.* **2020**, *11*, 1–10.
- [16] a) N. Yao, S. Y. Sun, X. Chen, X. Q. Zhang, X. Shen, Z. H. Fu, R. Zhang, Q. Zhang, *Angew. Chem. Int. Ed.* **2022**, *61*, e202210859; b) Q. Zhang, Y. Ma, Y. Lu, X. Zhou, L. Lin, L. Li, Z. Yan, Q. Zhao, K. Zhang, J. Chen, *Angew. Chem.* **2021**, *133*, 23545–23552; *Angew. Chem. Int. Ed.* **2021**, *60*, 23357–23364.
- [17] P. Sun, L. Ma, W. Zhou, M. Qiu, Z. Wang, D. Chao, W. Mai, *Angew. Chem. Int. Ed. Engl.* **2021**, *133*, 18395–18403.
- [18] S. Li, Y. Liu, L. Dai, S. Li, B. Wang, J. Xie, P. Li, *Energy Storage Mater.* **2022**, *48*, 439–446.
- [19] a) L. Miao, R. Wang, W. Xin, L. Zhang, Y. Geng, H. Peng, Z. Yan, D. Jiang, Z. Qian, Z. Zhu, *Energy Storage Mater.* **2022**, *49*, 445–453; b) S. Di, X. Nie, G. Ma, W. Yuan, Y. Wang, Y. Liu, S. Shen, N. Zhang, *Energy Storage Mater.* **2021**, *43*, 375–382.
- [20] Y. Fang, X. Xie, B. Zhang, Y. Chai, B. Lu, M. Liu, J. Zhou, S. Liang, *Adv. Funct. Mater.* **2022**, *32*, 2109671.
- [21] a) P. Zou, R. Zhang, L. Yao, J. Qin, K. Kisslinger, H. Zhuang, H. L. Xin, *Adv. Energy Mater.* **2021**, *11*, 2100982; b) Z. Xing, Y. Sun, X. Xie, Y. Tang, G. Xu, J. Han, B. Lu, S. Liang, G. Chen, J. Zhou, *Angew. Chem. Int. Ed.* **2022**, e202215324.
- [22] a) J. P. Perdew, K. Burke, M. Ernzerhof, *Phys. Rev. Lett.* **1996**, *77*, 3865; b) L. Y. Gan, Q. Zhang, Y. Cheng, U. Schwingenschlögl, *Phys. Rev. B* **2013**, *88*, 235310.
- [23] D. Dong, J. Xie, Z. Liang, Y. C. Lu, *ACS Energy Lett.* **2021**, *7*, 123–130.
- [24] T. G. Pattison, S. Wang, R. D. Miller, G. Y. Liu, G. G. Qiao, *Nat. Commun.* **2022**, *13*, 1–7.
- [25] N. Zhang, F. Y. Cheng, Y. C. Liu, Q. Zhao, K. X. Lei, C. C. Chen, X. S. Liu, J. Chen, *J. Am. Chem. Soc.* **2016**, *138*, 12894–12901.
- [26] K. Shi, Y. Lin, Z. Xiong, J. Li, S. Zhang, Q. Liu, *Chem. Eng. J.* **2022**, *430*, 132692.
- [27] J. Wang, Z. Zhao, G. Lu, Y. Zhang, Q. Kong, J. Zhao, G. Cui, *Mater. Today Energy* **2021**, *20*, 100630.
- [28] M. Zhao, Y. Lv, S. Zhao, Y. Xiao, J. Niu, Q. Yang, J. Qiu, F. Wang, S. Chen, *Adv. Mater.* **2022**, 2206239.
- [29] B. Tang, J. Zhou, G. Fang, F. Liu, C. Zhu, C. Wang, A. Pan, S. Liang, *J. Mater. Chem. A* **2019**, *7*, 940–945.
- [30] a) Z. Hu, F. Zhang, Y. Zhao, H. Wang, Y. Huang, F. Wu, R. Chen, L. Li, *Adv. Mater.* **2022**, *34*, 2203104; b) Z. Wu, M. Li, Y. Tian, H. Chen, S. J. Zhang, C. Sun, C. Li, M. Kiefel, C. Lai, Z. Lin, S. Zhang, *Nano-Micro Lett.* **2022**, *14*, 1–17; c) S. J. Zhang, J. Hao, D. Luo, P. F. Zhang, B. Zhang, K. Davey, Z. Lin, S. Z. Qiao, *Adv. Energy Mater.* **2021**, *11*, 2102010; d) W. Xu, K. Zhao, W. Huo, Y. Wang, G. Yao, X. Gu, H. Cheng, L. Mai, C. Hu, X. Wang, *Nano Energy* **2019**, *62*, 275–281; e) Y. Wu, Z. Zhu, D. Shen, L. Chen, T. Song, T. Kang, Z. Tong, Y. Tang, H. Wang, C. S. Lee, *Energy Storage Mater.* **2022**, *45*, 1084–1091; f) F. Wan, L. Zhang, X. Dai, X. Wang, Z. Niu, J. Chen, *Nat. Commun.* **2018**, *9*, 1–11; g) Y. Shang, P. Kumar, T. Musso, U. Mittal, Q. Du, X. Liang, D. Kundu, *Adv. Funct. Mater.* **2022**, *32*, 2200606; h) Y. Jiao, F. Li, X. Jin, Q. Lei, L. Li, L. Wang, T. Ye, E. He, J. Wang, H. Chen, J. Lu, R. Gao, Q. Li, C. Jiang, J. Li, G. He, M. Liao, H. Zhang, I. P. Parkin, H. Peng, Y. Zhang, *Adv. Funct. Mater.* **2021**, *31*, 2107652; i) D. Han, Z. Wang, H. Lu, H. Li, C. Cui, Z. Zhang, R. Sun, C. Geng, Q. Liang, X. Guo, Y. Mo, X. Zhi, F. Kang, Z. Weng, Q. H. Yang, *Adv. Energy Mater.* **2022**, *12*, 2102982.
- [31] G. Kresse, J. Hafner, *Phys. Rev. B* **1993**, *47*, 558.

Manuscript received: December 12, 2022

Revised manuscript received: January 13, 2023

Accepted manuscript online: January 21, 2023

Version of record online: January 26, 2023